SUPPLEMENTARY APPENDIX

Supplemental Figure 1. Histopathologic Characteristics of the Tumors in the Discovery Cohort

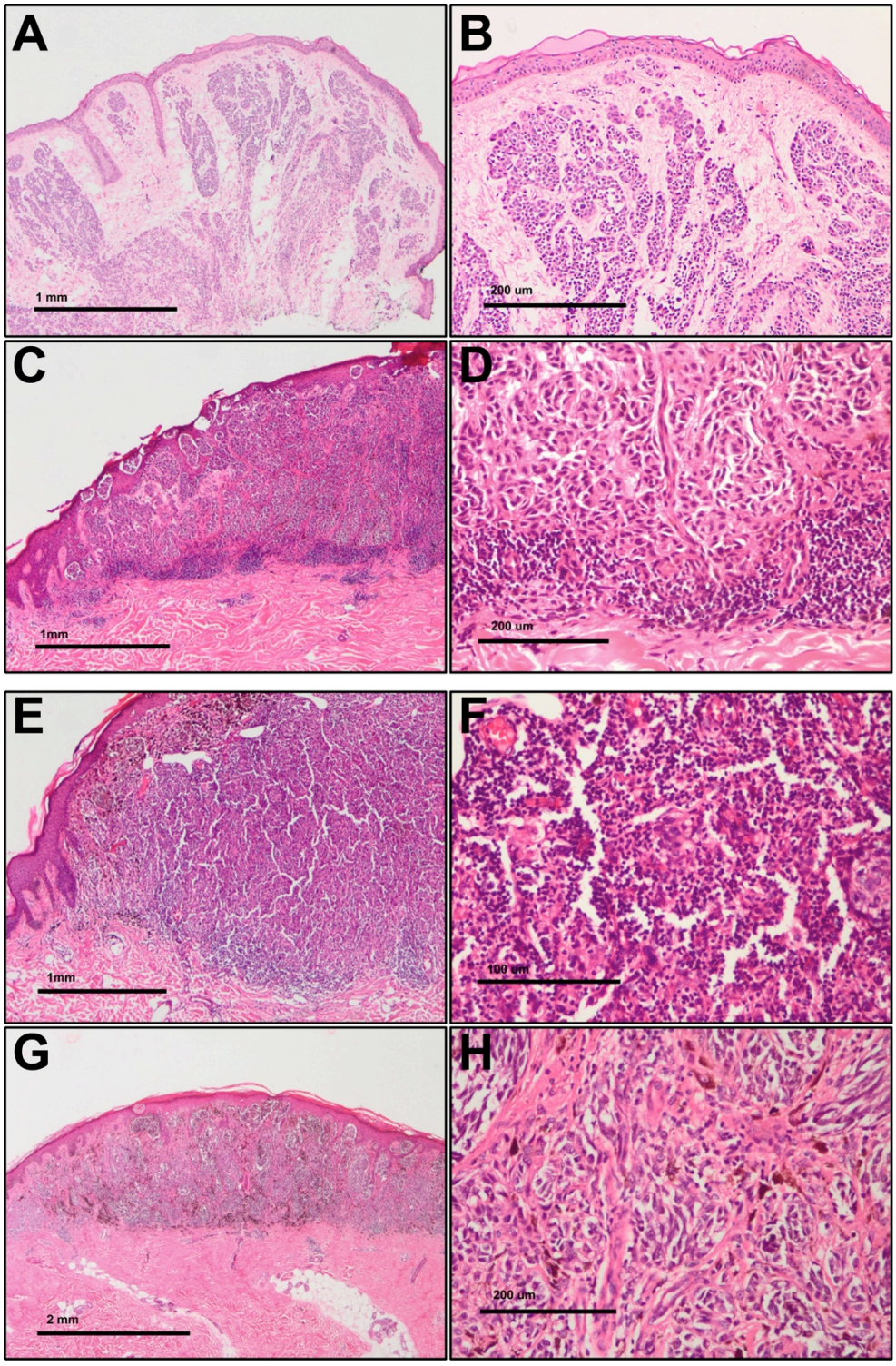

Figure S1. H&E staining of representative examples of the tumors samples within our cohort are shown. (**A, B**) Common acquired nevus (intradermal melanocytic nevus). (**C, D**) Primary melanoma, nodular type, with multifocal brisk tumor infiltrating lymphocytes located at the periphery. (**E, F**) Primary melanoma, nodular type, with segmental brisk tumor infiltrating lymphocytes throughout the entire neoplasm. (**G, H**) Primary melanoma, nodular type, with focal scattered non-brisk tumor infiltrating lymphocytes.

Supplemental Figure 2. Incorporation of Normal Epidermal Melanocytic Signature into Differential Gene Expression and Functional Pathway Analysis

Skin biopsies of melanocytic nevus and primary melanoma of the skin harbor cell types other than nevus and melanoma cells, respectively (i.e. epidermal keratinocytes and stromal cells). Moreover, nevus and melanoma cell contents vary across different samples. Although all our samples had an overlying epidermis and the nevus samples were selected to harbor large melanocytic content (compound and intradermal nevi), dissecting the transcriptional signal output of different cell types within human tumors can be challenging.

In order to measure the influence of variable melanocyte content on differential gene expression, we used the results of Reemann, *et al.* (1) and defined gene expression signatures of normal epidermal melanocytes (normal melanocytic signature, NMS) relative to dermal fibroblasts (FB), epidermal keratinocytes (KC) and whole skin (WS). Additionally, we utilized the RNA-sequencing data of the TCGA (http://cancergenome.nih.gov/) as well as RNA-sequencing of normal skin (NS-extremely low melanocytic content) and dysplastic compound nevus (DN-low melanocytic content) samples that were collected as a part of our study. We performed differential expression analysis using limma-voom for regional cutaneous metastasis (RCM), regional lymph node metastasis (RLNM), and distant metastasis to skin (DMs). For this analysis, we considered only genes with count per million > 10 in at least 20 samples. We considered only DEG with Benjamini-Hochberg corrected *P* value < 0.005 and a fold change > 1.5. We performed PCA plots to confirm effective differentiation of subtypes and annotated genes by melanocytic expression in the NMS.

For each pair of subtypes, we determined similarity of the set of differentially expressed genes (DEG) to the NMS. We confirmed that for all subtypes, our DEGs were significantly enriched for NMS genes by Fisher's exact test. We refer to the NMS genes present in our DEGs as NMS/DEG. We next examined whether the over- or under-expression of DEGs of a given subtype was aligned with the over-/under-expression of genes expressed on melanocytes. To this end, we compared the principal component analysis (PCA) plots of factor scores and loadings. For each pair of subtypes, the plot of the factor scores demonstrated that samples are clustered by subtype predominantly along the first component. Similarly, the corresponding plot of variable loadings also showed that all DEGs are clustered into over- and under-expressed groups of genes mostly along the first principal component. To better determine how well these genes clustered along the first principal component, we performed linear discriminant analysis on the variable loadings with differential expression by

subtype as a class label. The resulting linear discriminant describes a supervised projection of the genes that explicitly maximizes the distance between the centroids of the two classes, unlike PCA that preserves covariance and thereby clusters genes in an unsupervised manner. The decision boundary separating the two classes is orthogonal to the linear discriminant and is depicted in as a solid black line in Figure S2. A decision boundary that is also orthogonal to the first principal component indicates that the linear discriminant and the first principal component coincide, and that clustering by subtype is maximal along the first principal component.

For each comparison of subtypes, we determined whether the two clusters of over- and under-expressed DEGs coincided with the over- or under-expressed melanocytic genes. We inferred that clustering of over- or under-expressed NMS/DEG gene along the first principal component (or linear discriminant) would indicate that differential expression of that pair of subtypes is heavily influenced by the melanocytic content. Conversely, clustering of over- or under-expressed NMS/DEG genes along the second component (or linear discriminant decision boundary) would suggest that melanocytic content did not play an essential role in the differentiation between subtypes.

To quantify how strongly NMS/DEG genes contribute to each component, we considered the two distributions of over- or under-expressed NMS/DEG genes projected onto the given principal component. We calculated the corresponding Kolmogorov-Smirnov statistic KS_n as a measure for how much principal component *n* explains normal melanocytic expression in the two samples. Plotting KS1 and KS2 for each pair of subtypes revealed two distinct clusters, as highlighted by a minimum-distance decision boundary. In the dense cluster with high KS1 and low KS2, the first (and second) principal component maximally (and minimally) explained the differentiation of both subtypes (i.e. T4 vs. T1) and NMS (i.e. MC vs. WS). On the other hand, the second cluster characterized by either high KS2 or low KS1 included comparisons between PM vs. CAN, DN vs. NS, RCM vs. PM, and RLNM vs. PM. Similar results were found for KS statistics corresponding to the projected distribution of genes on the linear discriminant and orthogonal decision boundary. We therefore concluded that differential gene expression in subtype comparisons with high KS2 or low KS1 were not heavily influenced by the NMS, likely due to a smaller difference in the melanocytic cell content.

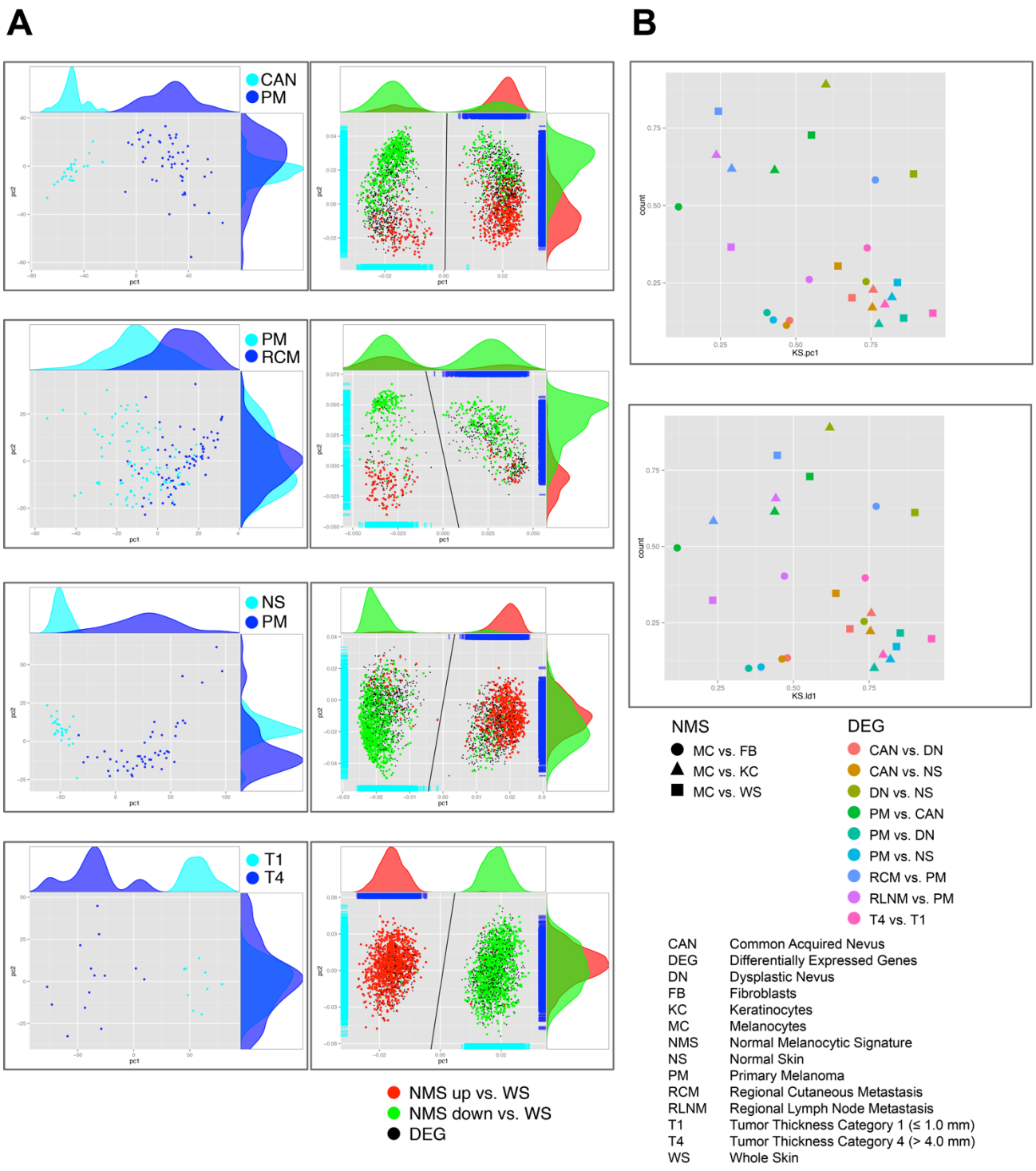

Figure S2. (**A**) Selected PCA plots of PM vs. CAN (first row), RCM vs. PM (second row), PM vs. NS (third row), and T4 vs. T1 (fourth row). Left column: Factor scores show clustering of samples by subtype. Right column: Variable loadings show clustering of genes by differential expression across subtype, with genes annotated by melanocytic expression in green and red. (**B**) Plot of Kolmogorov-Smirnov statistics (top) along the first and second principal components (bottom) along the linear discriminant and orthogonal decision boundary.

Supplemental Figure 3. Differentially Expressed Endogenous Elements between Melanoma vs. Nevus Subsets

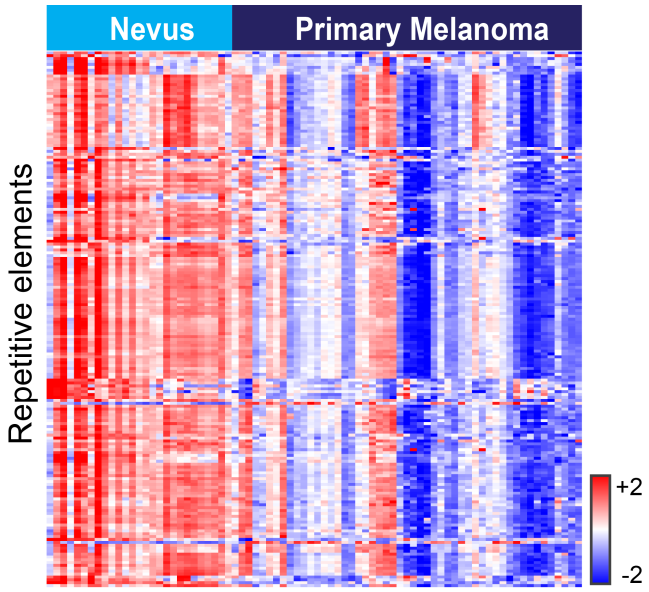

Figure S3. Heatmap represents differentially expressed noncoding repetitive element transcripts (endogenous retroviruses (ERVs), short interspersed nuclear elements (SINEs), and long interspersed nuclear elements (LINEs).

Supplemental Figure 4. Identification of the Epgn3 (high-risk) Cluster in Independent Melanoma Datasets

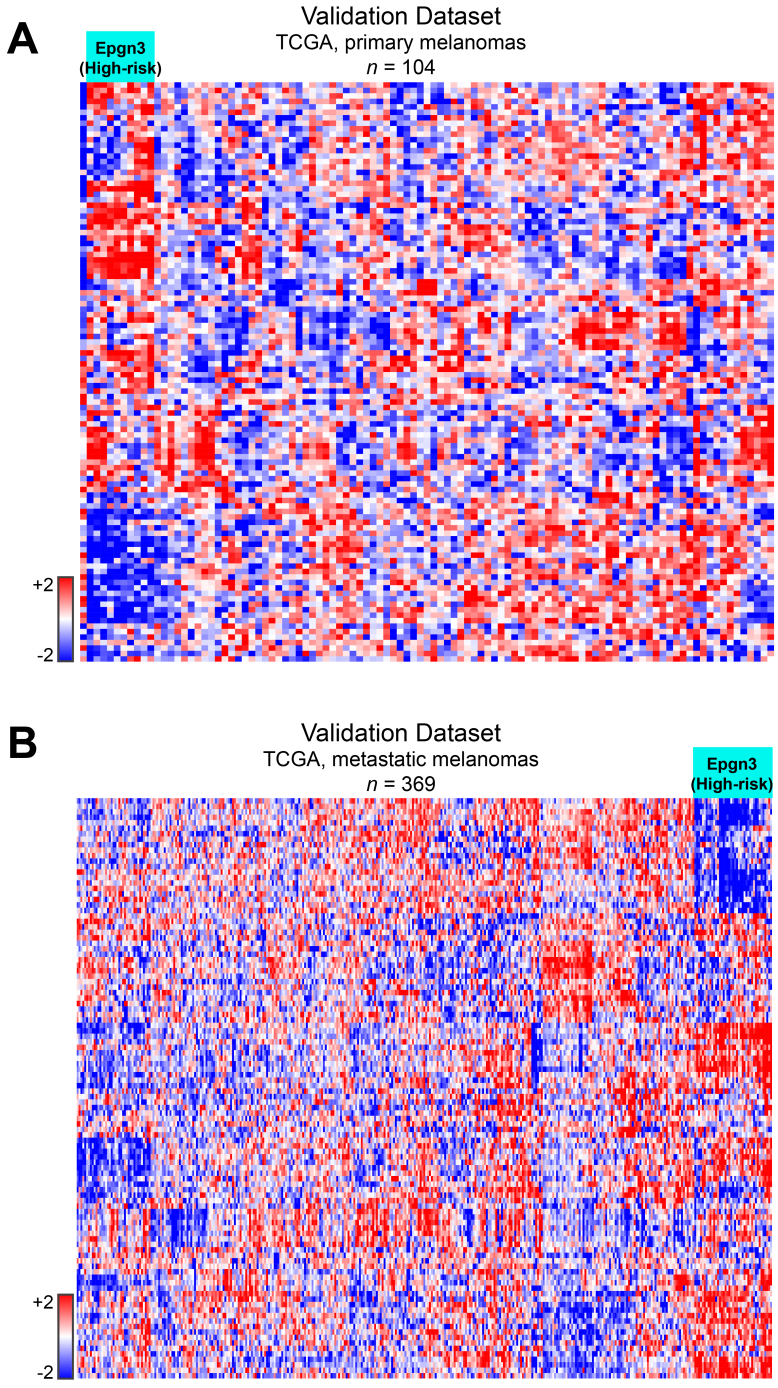

Figure S4. TCGA dataset of melanomas (*n* = 473) were downloaded from https://cancergenome.nih.gov/. (**A**) and (**B**) Samples were selected based on sample type as 'primary' tumor or 'metastasis'. TMM normalization was utilized across the samples. Heatmaps represent unsupervised hierarchical clustering of the tumor samples using the 122-epigenetic gene signature.

Supplemental Figure 5. Prognostic Significance of the 122-Epigenetic Gene Signature on Patient Survival

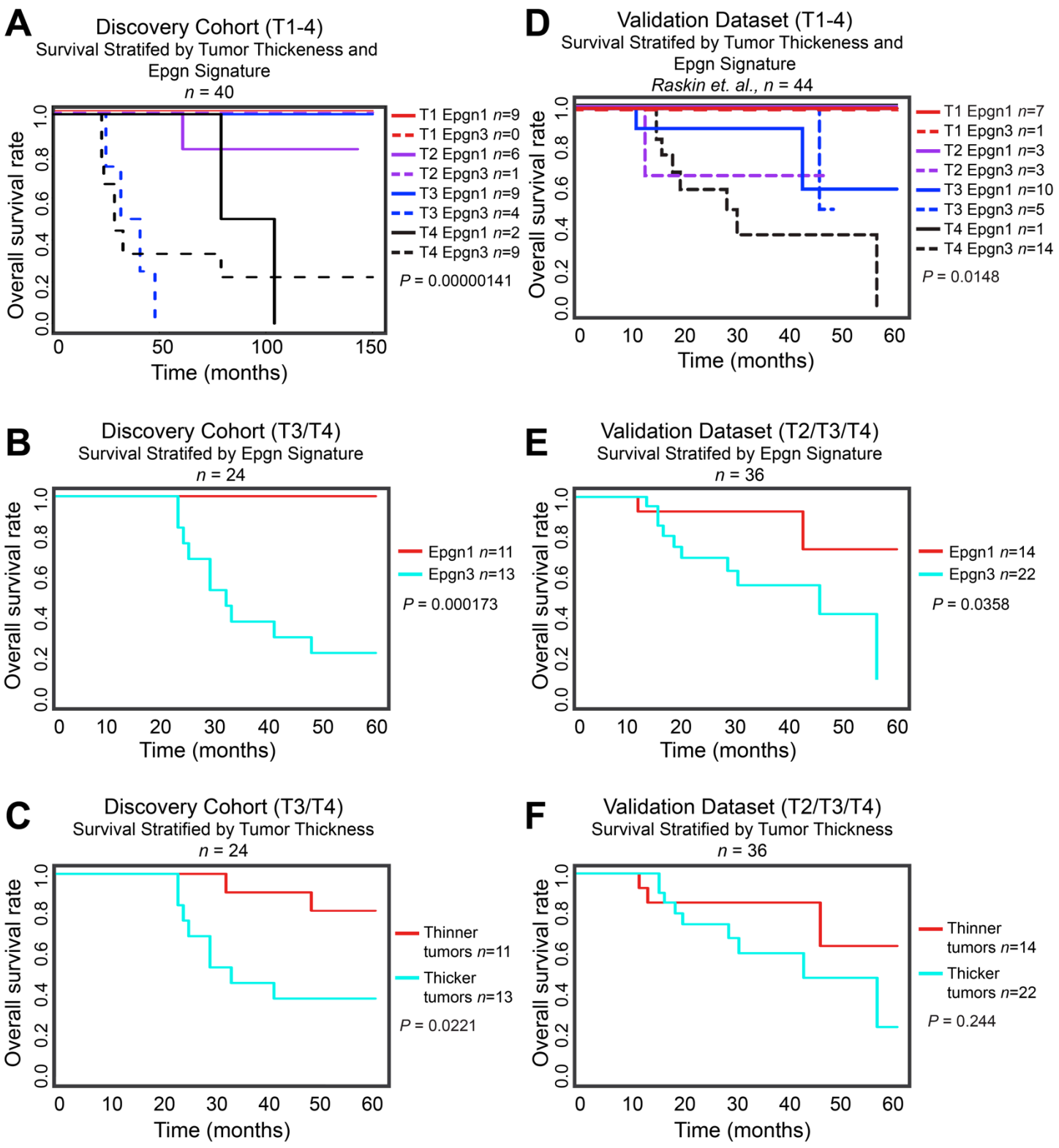

Figure S5. (**A**) The discovery cohort consisted of 51 primary melanoma patients. We excluded the outlier group that consisted of a few number of cases (Epgn2 group, *n* = 6) and examined the resultant 45 patients that clustered within either Epgn1 (low-risk) or Epgn3 (high-risk) groups. Survival outcome data was available in forty of the 45 patients. Relatively thin tumors (T1/T2) fell mostly in the Epgn1 group (Epgn1 *n* =15, Epgn3 *n* =1) whereas the thicker tumors (T3/T4) had a uniform distribution of Epgn1 (*n* =11) and Epgn3 (*n* =13) samples. (**B**) Thus, we first examined the 5-year survival of T3/T4 cases stratified by the Epgn1/3 classification and found a significant prognostic value on patient outcomes (*P* = 0.000173). Of importance, none of the patients in the Epgn1 (low-risk) group died within this time frame. (**C**) When the 5-year survival rates of T3/T4 patients were stratified by tumor thickness categories (thinner tumors *n* =11, thicker tumors *n* =13), as expected, we found that tumor thickness showed a significant prognostic value (*P* = 0.0221). Of note, some patients in the Epgn1 group (low-risk) died within the 5-year time interval. (**D**-**E**) Similar analysis was applied to the external dataset (2). Relatively thin tumors (T1) consisted of Epgn1 cases (Epgn1 *n* =7, Epgn3 *n* =1), whereas the thicker tumors (T2/T3/T4) had a uniform distribution (Epgn1 *n* =14, Epgn3 *n* =22). When stratified either by Epgn1/3 or tumor thickness categories, Epgn1/3 classification performed better in predicting patient outcome (*P* = 00358); all patients in the Epgn3 group died within this interval. Log-rank test was used for the analyses.

Supplemental Figure 6. *TP53*, *TP63*, and *TP73* Correlate with *LINE1* and the Epigenetic Signature

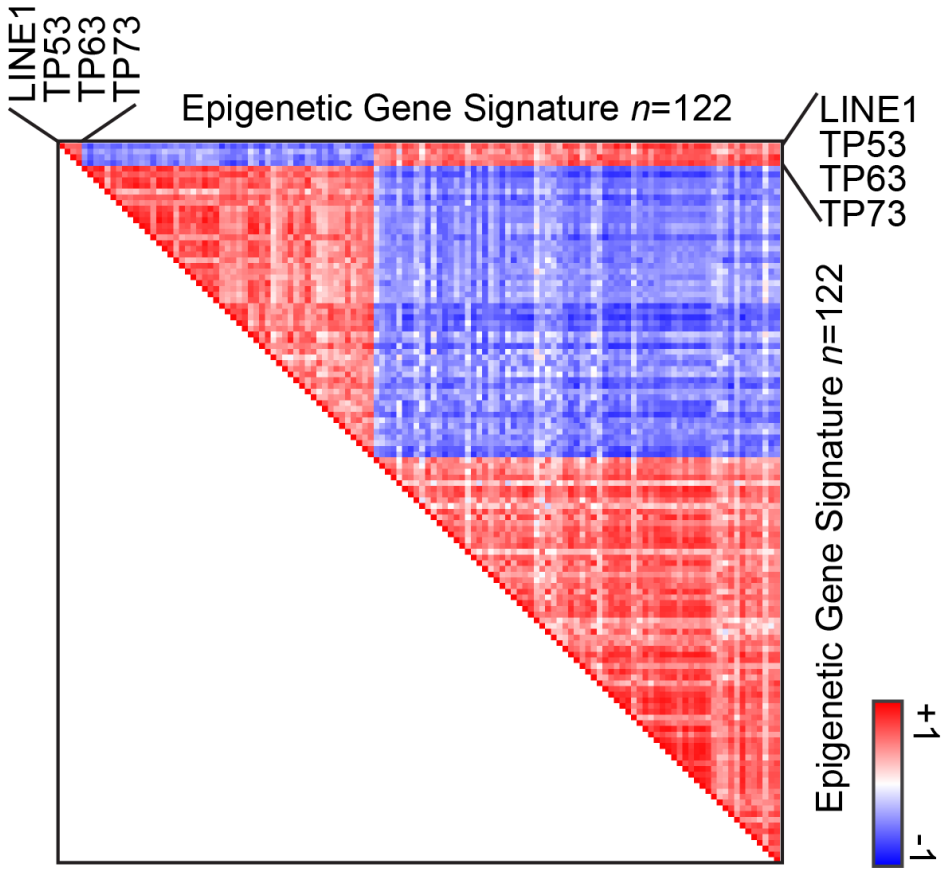

Figure S6. Expression correlation matrix of 126 total genes in primary melanoma samples from the discovery cohort (Epgn1 and Epgn3 samples, *n* = 45). Positive correlation is indicated by increasing red color and negative correlation by increasing blue color intensity.

1. Reemann, P., et al. 2014. Melanocytes in the skin--comparative whole transcriptome analysis of main skin cell types. *PLoS One* 9:e115717.
2. Raskin, L., et al. 2013. Transcriptome profiling identifies HMGA2 as a biomarker of melanoma progression and prognosis. *J Invest Dermatol* 133:2585-2592.